Supplemental Table 1: Clinical and demographic features of MS and nonMS patients.

	MS (n=14)	nonMS (n=10)	*p* value*
Mean age (range, yrs.)	60 (25-80)	62 (36-77)	NS
M:F	6:8	5:5	NS
Disease phenotype	PP-MS[1] (n=3) RR-MS[2] (n=2) SP-MS[3] (n=9)	Stroke (n=1), drug overdose (n=1), nonCNS disease (cancer n=2, sepsis n=2, myocardial infarction n=2, HIV/AIDS n=2)	
Disease Duration (range, yrs.)	5-20	1-5	
Therapy	DMT (n=2)[4]	(cancer chemotherapy, n=3; antibiotics, n=1)	
EDSS	5.0-9.5	N/A	

* non-significant (NS)
[1] Primary Progressive MS
[2] Relapsing-remitting MS
[3] Secondary Progressive MS
[4] IFN-beta and glatiramer acetate

Supplementary Table 1: Mouse primer sequences

Gene Name	Species	Sequence
nlrp3	mouse	5’-ATT ACC CGC CCG AGA AAG G-3’ 5’-TCG CAG CAA AGA TCC ACA CAG-3’
casp1	mouse	5’-ACA AGG CAC GGG ACC TAT G-3’ 5’-TCC CAG TCA GTC CTG GAA ATG-3’
il1b	mouse	5’-GCA ACT GTT CCT GAA CTC AAC T-3’ 5’-ATC TTT TGG GGT CCG TCA ACT-3’
il18	mouse	5'-ACT TTG GCC GAC TTC ACT GT-3’ 5'-GGG TTC ACT GGC ACT TTG AT-3'
asc	mouse	5’-CTT GTC AGG GGA TGA ACT CAA AA-3’ 5’-GCC ATA CGA CTC CAG ATA GTA GC-3’
aim2	mouse	5’-GTC ACC AGT TCC TCA GTT GTG -3’ 5’- CAC CTC CAT TGT CCC TGT TTT AT-3’
nlrp1a	mouse	5’-ACA GAC ATG GAC CTC ATG GTG GTT-3’ 5’-CAA CTC CTC CAG GTT TCT GGC TAA C-3’
nlrp6	mouse	5'-TCT TTT GCT TGC CCT TCT GT-3’ 5'-AGC CCA AAG TCC CTC TGA AT-3
nlrp2	mouse	5'-CAT GCC AAC ACT TCC TCC TT-3’ 5'-ACG GTC CAC TTT CTG TTT GG-3'
pyrin	mouse	5'-CCC TAC TGG ATG AGA TGA TTG AAG AAC-3’ 5'-TCC AAC AGC TCA GAG GCA GAC AT-3'
casp11	mouse	5'-AGA GGG CAT GGA GTC AGA GA-3’ 5'-GCC ATG AGA CAT TAG CAC CA-3'
nlrc4	mouse	5'-AAT TCA GAT GGG CAG ACA GG-3’ 5'-TCA CCT GAA GCT CCA CCT CT-3'
cd3e	mouse	5'-GAT GCA GTC GGG CAC TCA CT-3’ 5'-CAT TAC CAT CTT GCC CCC AA-3'
tnfa	mouse	5'-CAT CTT CTC AAA ATT CGA GTG ACA A-3’ 5'-TGG GAG TAG ACA AGG TAC AAC CC-3'
f480	mouse	5'-GCT GTG AGA TTG TGG AAG CA-3’ 5'-AGT TTG CCA TCC GGT TAC AG-3'
ifng	mouse	5'-GCA TTC ATG AGT ATT GCC AAG-3’ 5'-GGT GGA CCA CTC GGA TGA-3'
hprt	mouse	5'-AGC CTA AGA TGA GCG CAA GT-3’ 5'-TTA CTA GGC AGA TGG CCA CA-3'

Supplementary Table 2: Human primer sequences

Gene Name	Species	Sequence
NLRP3	human	5’-GAT CTT CGC TGC GAT CAA CAG-3’ 5’-CGT GCA TTA TCT GAA CCC CAC-3’
CASP1	human	5’-TCC AAT AAT GGA CAA GTC AAG CC-3’ 5’-GCT GTA CCC CAG ATT TTG TAG CA-3’
IL1B	human	5’-CCA AAG AAG AAG ATG GAA AAG C-3’ 5’-GGT GCT GAT GTA CCA GTT GGG-3’
IL18	human	5’- TCT TCA TTG ACC AAG GAA ATC GG-3’ 5’-TCC GGG GTG CAT TAT CTC TAC-3’
ASC	human	5’-GCC TGC ACT TTA TAG ACC AGC-3’ 5’-GCT TCC GCA TCT TGC TTG G-3’
AIM2	human	5’-TCA AGC TGA AAT GAG TCC TGC-3’ 5’-CAC GTT GCT TTG CGA CAT CA-3’
NLRP1	human	5’-ATT CCA GTT TGT GCG AAT CCA-3’ 5’-GTT CCT TGG GGA GTA TTT CCA G-3’
NLRP2	human	5'-ATG CAC CGA ATG GAT CTG TC-3’ 5'-CGT TCT TTC CGT GTT ATC CC-3’
PYRIN	human	5'-GGC TAA GAC AGT GCC T-3’ 5'-GGT AAG CGG TTT CTG C-3'
CASP4	human	5’-CAA GAG AAG CAA CGT ATG GCA-3’ 5’-AGG CAG ATG GTC AAA CTC TGT A-3’
NLRC4	human	5’-TGC ATC ATT GAA GGG GAA TCT G-3’ 5’-GAT TGT GCC AGG TAT ATC CAG G-3’
TRADD	human	5’-GCT GTT TGA GTT GCA TCC TAG C -3’ 5’-CCG CAC TTC AGA TTT CGC A -3’
FADD	human	5’-TCT CCT CTC TGA GAC TGC TAA G-3’ 5’-AGA GAG TGC TGT GTG TCA ATC-3’
CASP8	human	5’-AGT AAG CAA CAA GGA TGA CAA GA-3’ 5’-ATC AAT CAG AAG GGA AGA CAA GTT-3’
TRAF2	human	5’-CAC ACC TGT CCC TCT TCT TTG-3’ 5’-CCT GAA GGC GTC AAT CAC GTG-3’
GAPDH	human	5’-AGC CTT CTC CAT GGT GGT GAA GAC-3’ 5’-CGG AGT CAA CGG ATT TGG TCG -3’

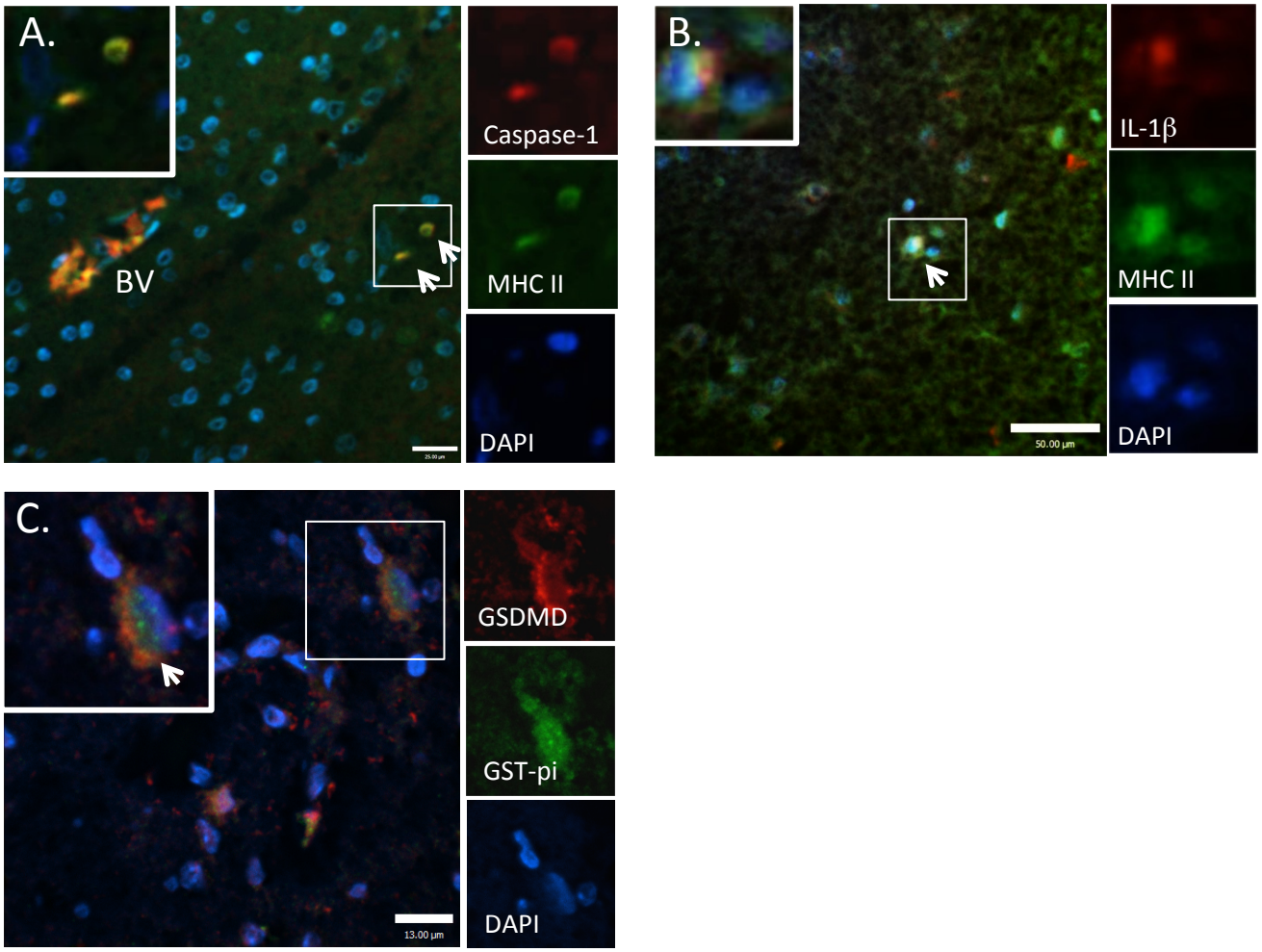

Supplemental Figure 1: Expression of inflammasome proteins in multiple CNS cell types
(A) Immunofluorescent labeling of MS white matter demonstrates that IL-1β immunoreactivity (inset, red) is observed in cells that are immunopositive for MHC Class II (green, overlap appears yellow), both in the CNS parenchyma and within blood vessels (indicated BV). Scale bar = 35.00µm. (B) Caspase-1 immunoreactivity (inset, red) was detected in cells that are immunopositive for MHC Class II molecules (green; overlap shown in yellow). Scale bar = 50.00µm. (C) GSDMD was detected in cells that are GST-pi immunopositive and display nuclear disintegration (DAPI). Scale bar = 13.00µm.

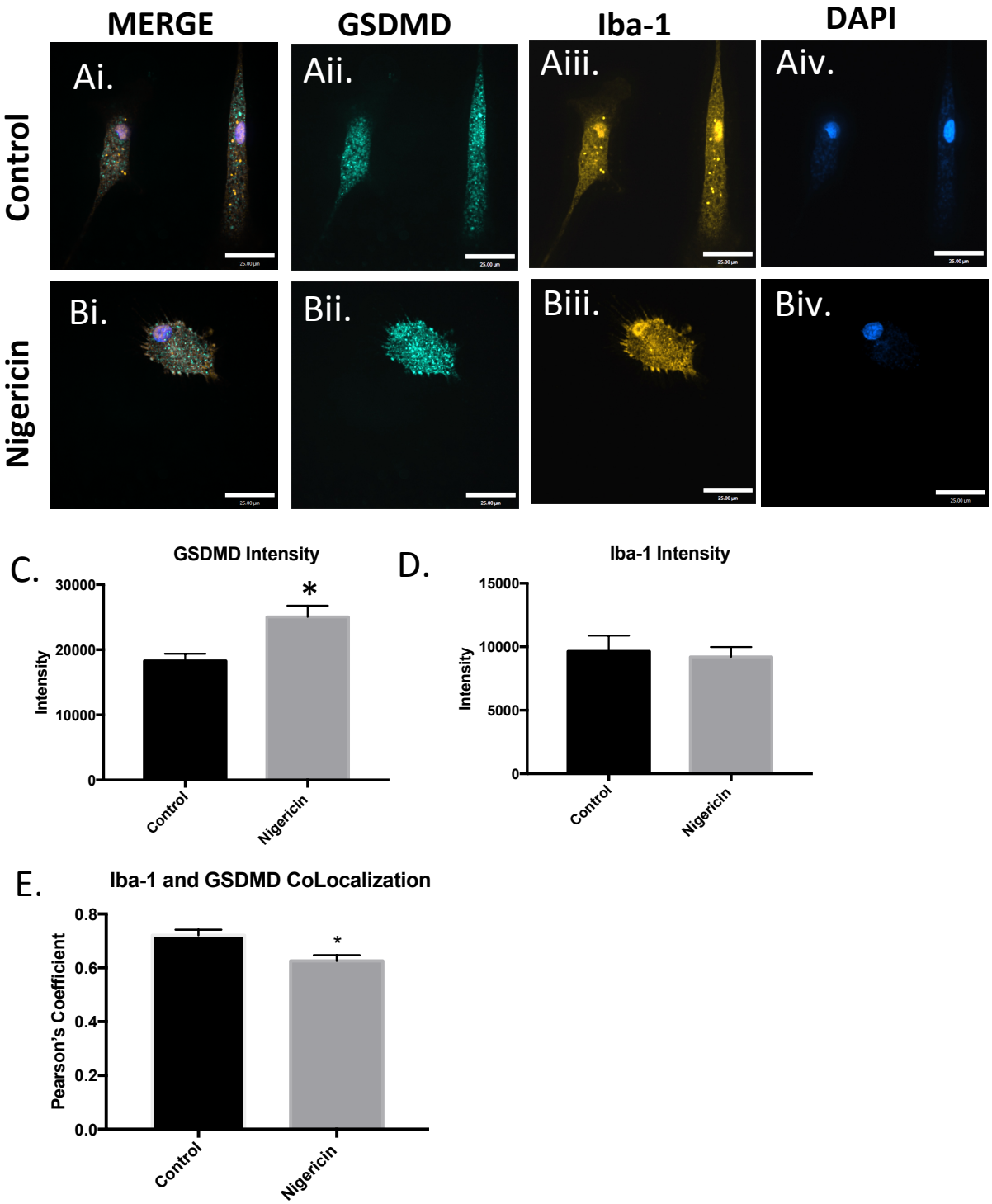

Supplemental Figure 2: Iba-1 expression in nigericin-exposed microglia
Human microglia were exposed to (A) PBS control or (B) nigericin (5μM) for 4hrs and assessed for Iba-1 and GSDMD immunoreactivity. (C) GSDMD intensity increased significantly with nigericin exposure (Student's *t*-test, $p<0.05$,) while Iba-1 intensity remained unchanged. (E) Co-expression of Iba-1 and GSDMD was assessed using Pearson's coefficient. Nigericin treatment caused a significant decrease in co-expression (Pearson's Coefficient, $p<0.05$). A minimum of 30 cells were individually characterized for each experimental condition.

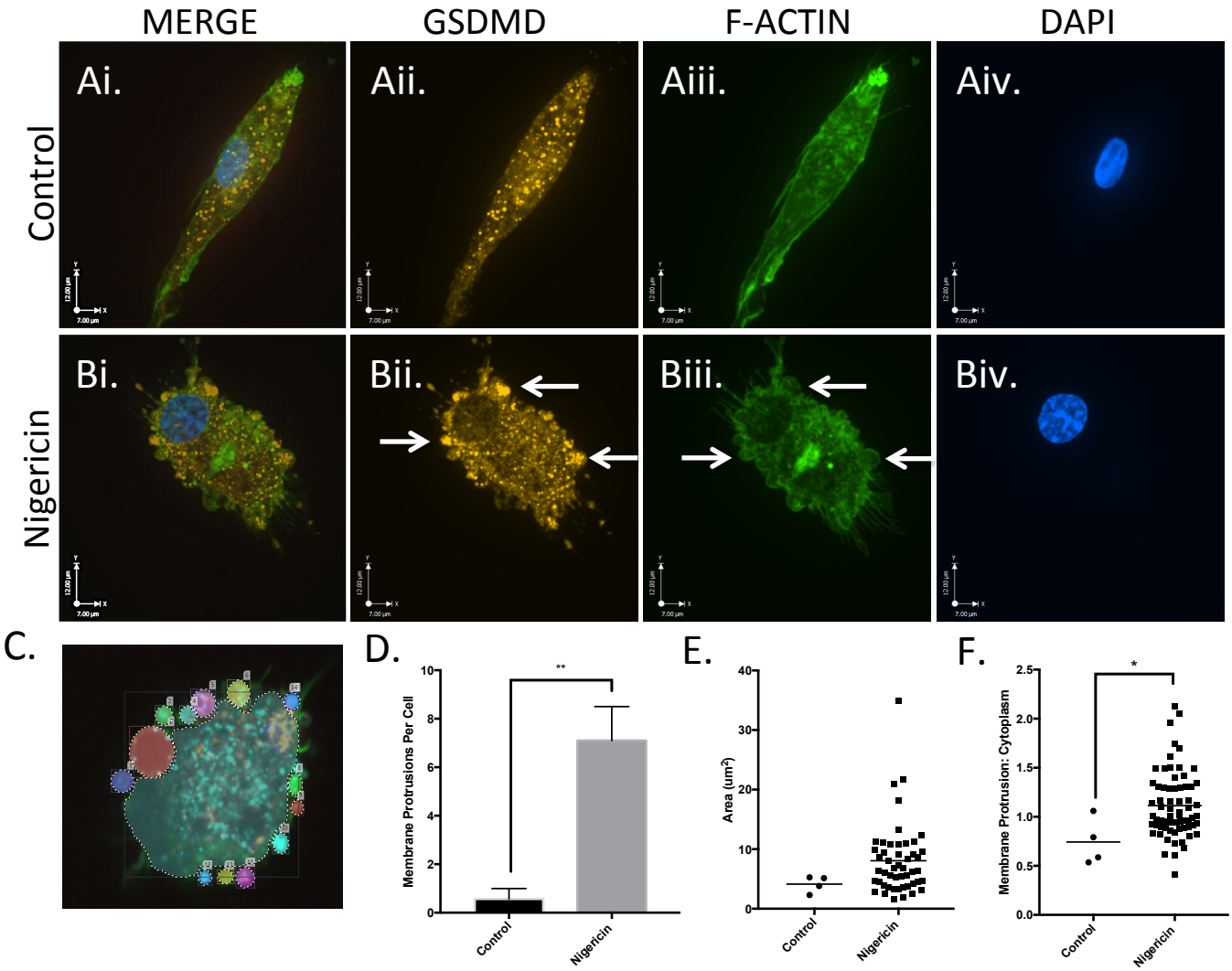

Supplemental Figure 3: Formation of GSDMD$^+$ pyroptotic bodies during microglial pyroptosis
(A) Immunofluorescent imaging of human microglia reveal intact processes (Aiii) and diffuse GSDMD staining (Aii). Nigericin exposure causes the loss of processes and formation of GSDMD-positive cell membrane protrusions (Bii, Biii, arrows) corresponding to pyroptosis-associated local osmotic stress and swelling. Horizontal scale axis = 7μm and vertical scale axis = 12μm. (C) Image from Volocity 6.3 analysis software demonstrating quantification procedure for pyroptotic bodies on nigericin-treated microglia. Quantification of pyroptotic bodies was performed by selecting a circular region of interest (ROI) overlaying each pyroptotic body and measuring mean fluorescence intensity (MFI) and area (μm^2) of each pyroptotic body individually. MFI of the cytoplasm was calculated by selecting an ROI within the cell body that excluded membrane and pyroptotic bodies. (D) The number of pyroptotic bodies identified on a subset of nigericin-treated microglia demonstrating the ring of fire phenotype was compared to that of control microglia. Data represent mean ± SEM and were tested for significance using Student's *t*-test. (E) Size of membrane protrusions was calculated for nigericin-treated microglia and compared for point of reference to the small number of membrane protrusions normally visible on untreated control cells. The area of pyroptotic bodies on microglia was observed to be 8.1± 0.9 μm^2. Each data point corresponds to an individual pyroptotic body. (F) The ratio of GSDMD immunoreactivity in each pyroptotic body compared to the cytoplasm was calculated by dividing the MFI of each pyroptotic body by the MFI of the cytoplasm. Each data point corresponds to an individual pyroptotic body (Student's *t*-test, *p<0.05, **p<0.01).

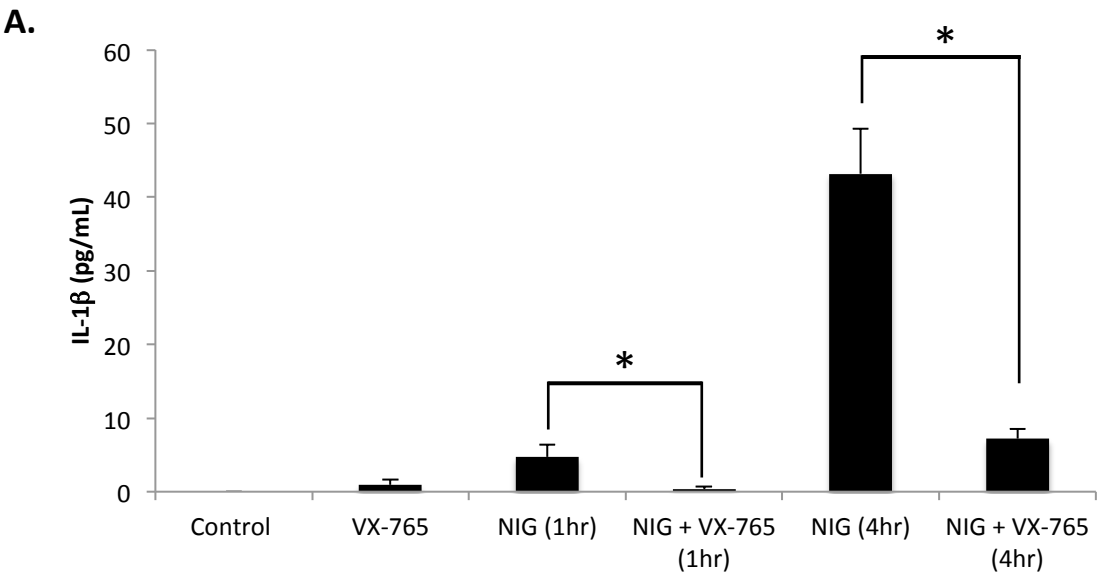

Supplemental Figure 4: Time-course of IL-1β release immediately following nigericin exposure
(A) Human microglia were exposed to nigericin (5μM) with or without 4hr pre-treatment with VX-765 (50μM), and supernatants harvested at 1 and 4hr post-exposure. IL-1β release was assessed by ELISA (technical replicates of 6 wells per condition). Il-1β levels significantly increased over time (Student's *t*-test; **p*<0,05,) and were reduced with VX-765 at both time points tested. Data represent mean ± SEM. ELISA shown is a representative example of experimental results independently replicated in three different tissue donors.

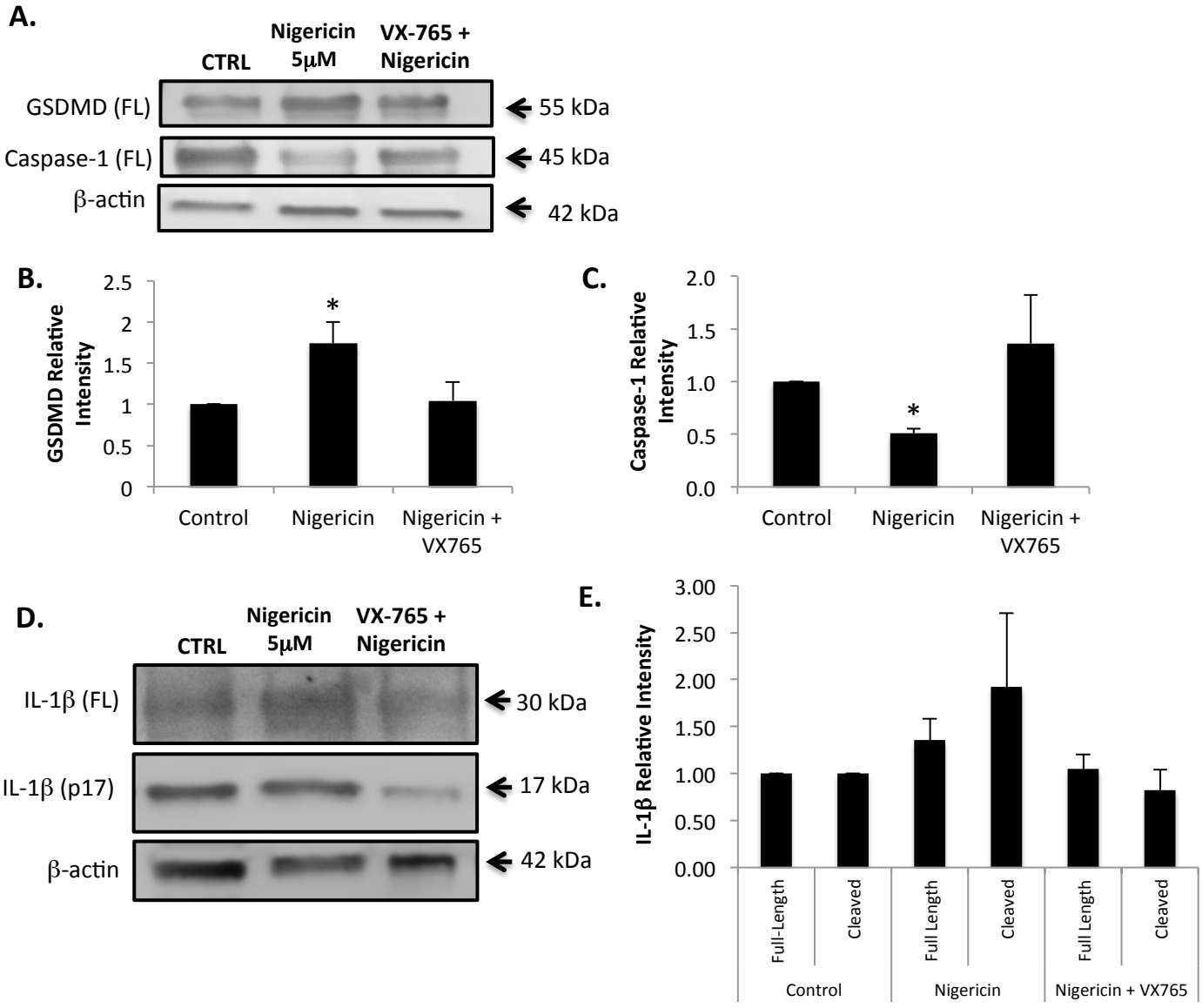

Supplemental Figure 5: Expression of inflammasome proteins in nigericin-exposed microglia
(A-C) Immunoblotting demonstrates an increase in the expression of full-length GSDMD and a decrease in the expression of full-length caspase-1 in lysates of microglia exposed to nigericin (4hrs), which was not observed following pre-treatment with VX-765 (50μM) prior to nigericin exposure. Data shown represent mean ± SEM of protein band intensities normalized to β-actin from at least two separate microglial donors (Student's *t*-test, **p*<0.05). (D-E) Nigericin exposure caused a trend towards an increase in both full-length and cleaved IL-1β immunoreactivity, which was not observed in cells that were pre-treated with VX-765 prior to nigericin exposure. Data shown represent mean ± SEM of protein band intensities normalized to β-actin from three different tissue donors.

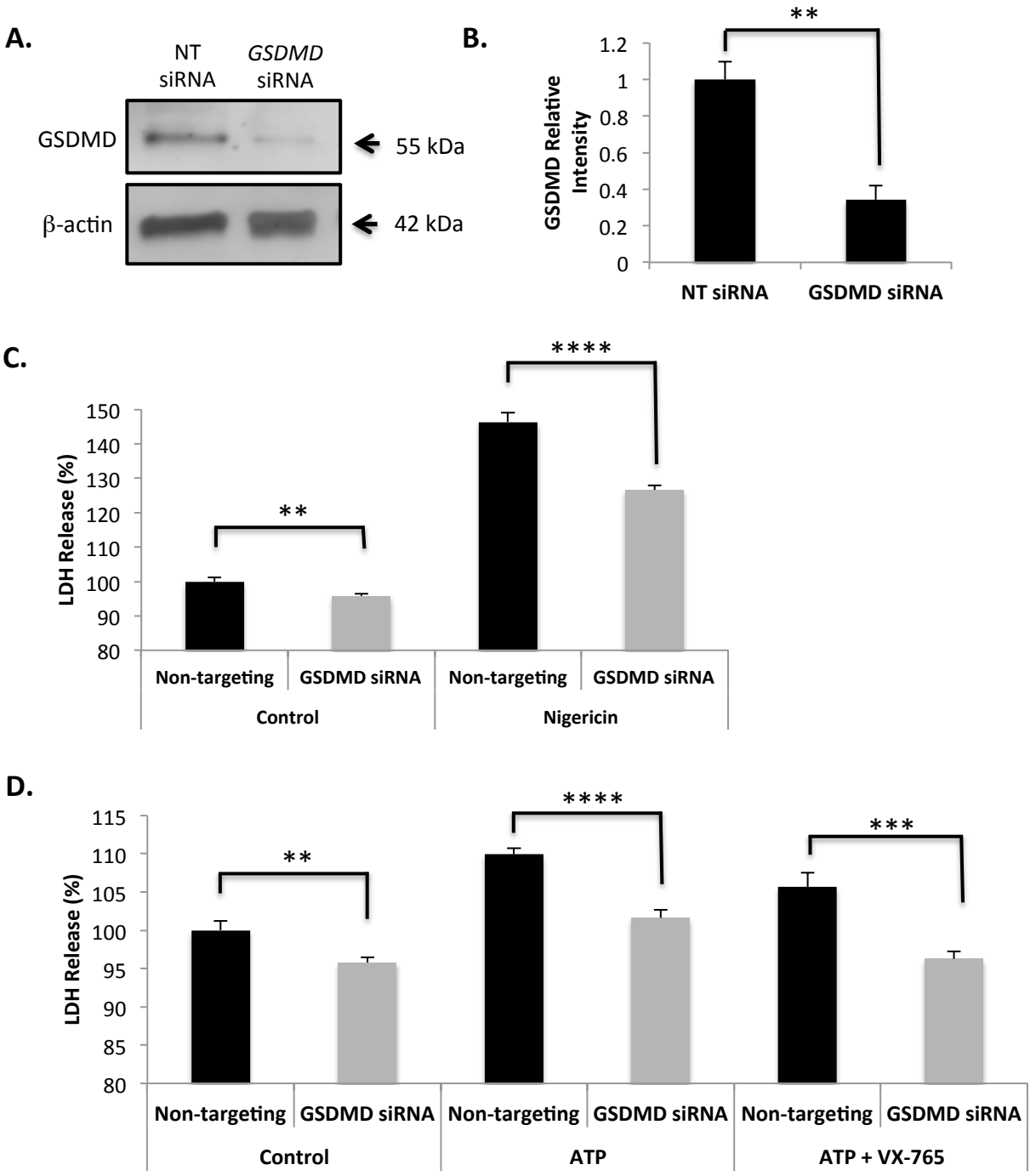

Supplemental Figure 6: siRNA-mediated knock-down of *GSDMD* in microglia

(A) Human microglia were transfected in 6-well plates with either non-targeting siRNA (NT siRNA) or pooled *GSDMD*-targeting siRNAs (*GSDMD* siRNA) for 48hrs. Protein was extracted from three replicate wells, pooled, and GSDMD protein expression assessed by Western blot. GSDMD siRNA-transfected cells showed a substantial reduction in GSDMD expression (representative Western blot shown). B) GSDMD intensity from four biologically unique donors was assessed by Western blot and normalized to β-actin. Data shown represent mean ± SEM (Student's *t*-test, *p<0.05, ** p<0.01). (C) Human microglia were transfected in 96-well plates with either non-targeting siRNA or with pooled *GSDMD*-targeting siRNAs for 48hrs. Microglia were then exposed to 5μM nigericin for 24hrs. Supernatant LDH activity levels (expressed as percent of untreated non-targeting siRNA-transfected controls) were assessed (8-12 technical replicates per condition). *GSDMD* siRNA-transfected cells released significantly less LDH activity (Student's *t*-test, ** p<0.01, **** p<0.0001). (D) *GSDMD* siRNA or non-targeting siRNA-transfected cells were exposed to 200μM ATP ± 50μM VX-765 (4hr pre-treatment) and supernatant LDH activity assessed. *GSDMD* siRNA-transfected cells released significantly less LDH following ATP exposure (Student's *t*-test, p<0.05). VX-765 treatment in conjunction with *GSDMD*-targeting siRNA completely prevented LDH release in ATP-exposed cells. All LDH assays shown are representative examples of experimental results independently replicated in three to four different tissue donors.

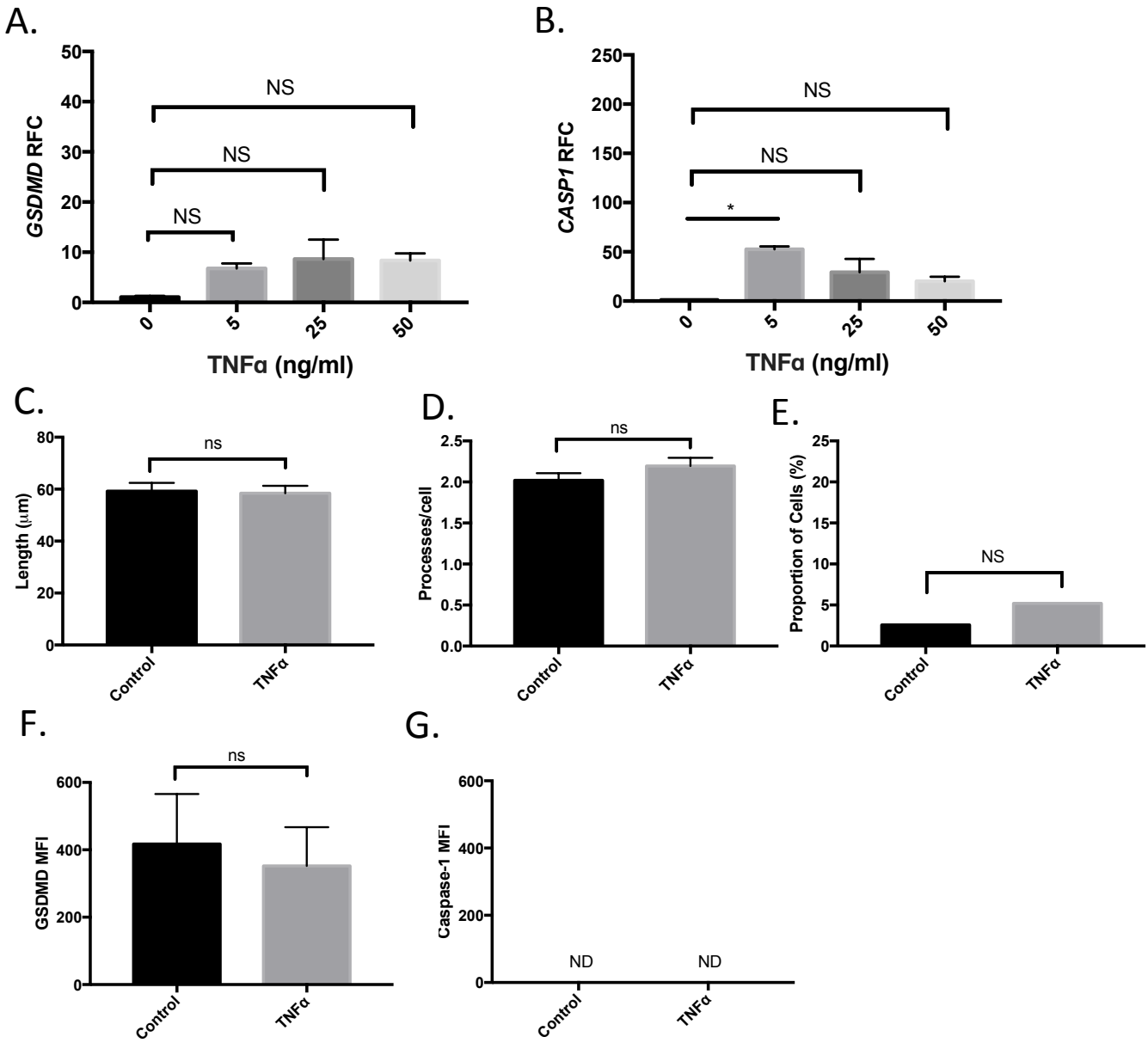

Supplemental Figure 7: Response of oligodendrocyte progenitor cells to TNFα exposure

Transcript levels of *GSDMD* (A) and *CASP1* (B) were assessed in undifferentiated oligodendrocyte progenitors (growth factor positive) in response to TNFα exposure (50ng/mL, 24hr). Values represent relative fold change (RFC) compared to untreated controls, with threshold cycles normalized to GAPDH (minimum of three technical replicates per condition; data represent mean ± SEM, tested for significance using 1-way ANOVA. To quantify morphological changes, the length (C) and number (D) of processes on each oligodendrocyte progenitor was quantified for a minimum of 100 cells per condition. Data shown represent mean ± SEM, tested for significance using Kruskal-Wallis test. (E) The proportion of dysmorphic oligodendrocyte progenitors in each treatment condition was quantified using a strict inclusion criteria: (i) condensed nucleus (ii) few or no processes (iii) positive for both f-actin and DAPI. A minimum of 100 cells were classified as either "healthy" or "dysmorphic" in each condition. The proportion of healthy versus dysmorphic oligodendrocyte progenitors in each condition was compared (Chi-square test). The mean fluorescence intensity (MFI) in the GSDMD (Cy5) and caspase-1 (FITC) channels was quantified in each treatment condition. Each oligodendrocyte cell body was individually outlined as a region of interest (ROI) and MFI measured for a minimum of 100 cells per condition. Background fluorescence was subtracted. Data shown represent MFI per cell (Kruskal-Wallis test, mean ± SEM).

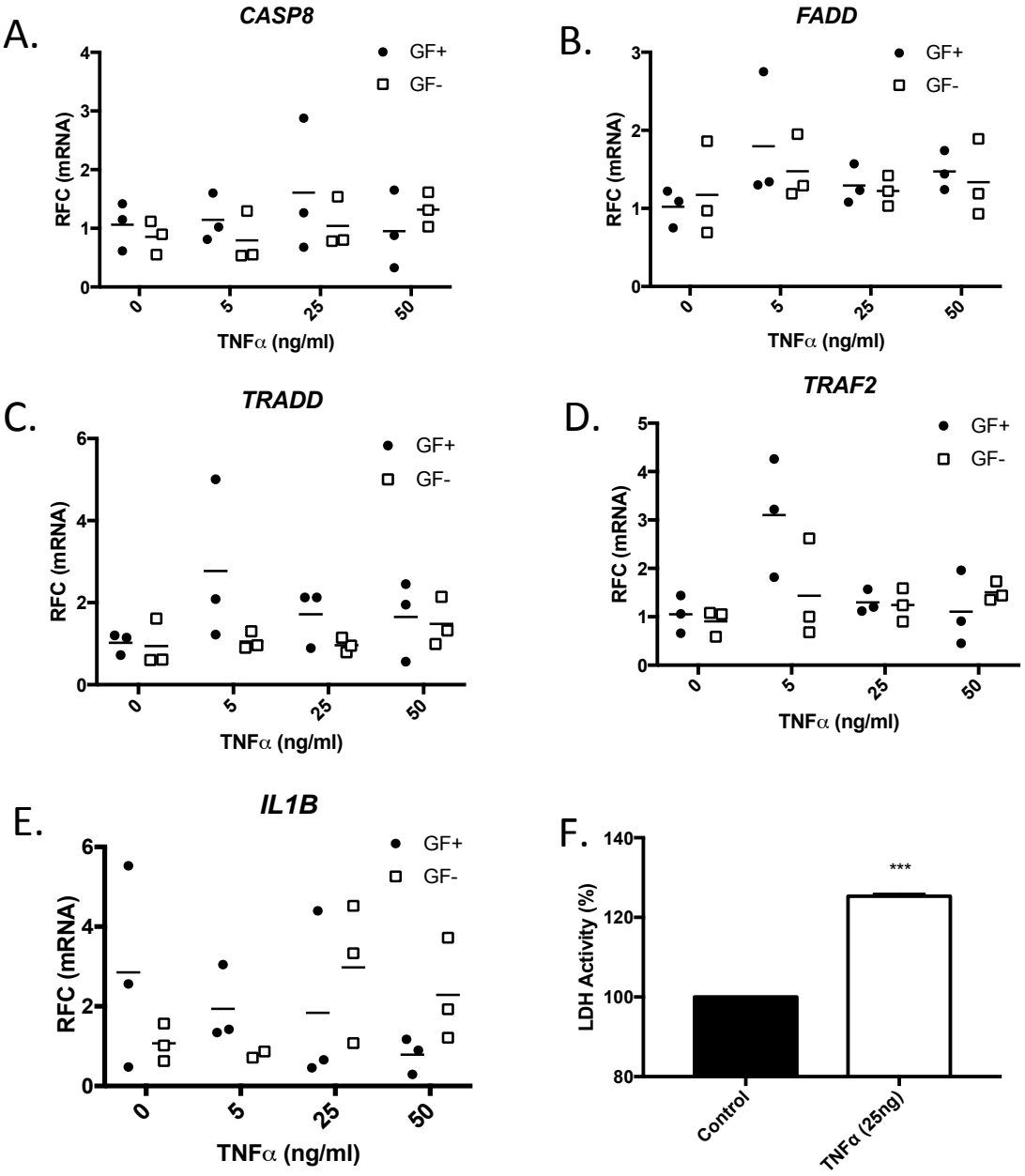

Supplemental Figure 8: Evidence for non-apoptotic cell death in TNFα-exposed ODCs
Differentiated oligodendrocytes (GF-) and undifferentiated progenitors (GF+) were exposed to increasing concentrations of TNFα as indicated and cell lysates were harvested 24hrs post-exposure. Transcript levels of genes related to the extrinsic apoptosis pathway, including (A) *CASP8*, (B) *FADD*, (C) *TRADD*, and (D) *TRAF2* were assessed via RT-PCR. Data represented are raw values for relative-fold change. Cells were differentiated for three days prior to TNFα exposure. (E) Differentiated and undifferentiated ODCs were exposed to increasing concentrations of TNFα and *IL1B* transcript levels assessed by RT-PCR. Data represented are raw values for relative-fold change. (F) Supernatant LDH activity in TNFα-exposed differentiated ODCs was measured 24hrs post-treatment and normalized to untreated controls. Cells were differentiated for seven days prior to TNFα exposure (Student's *t*-test, ***$p<0.001$).

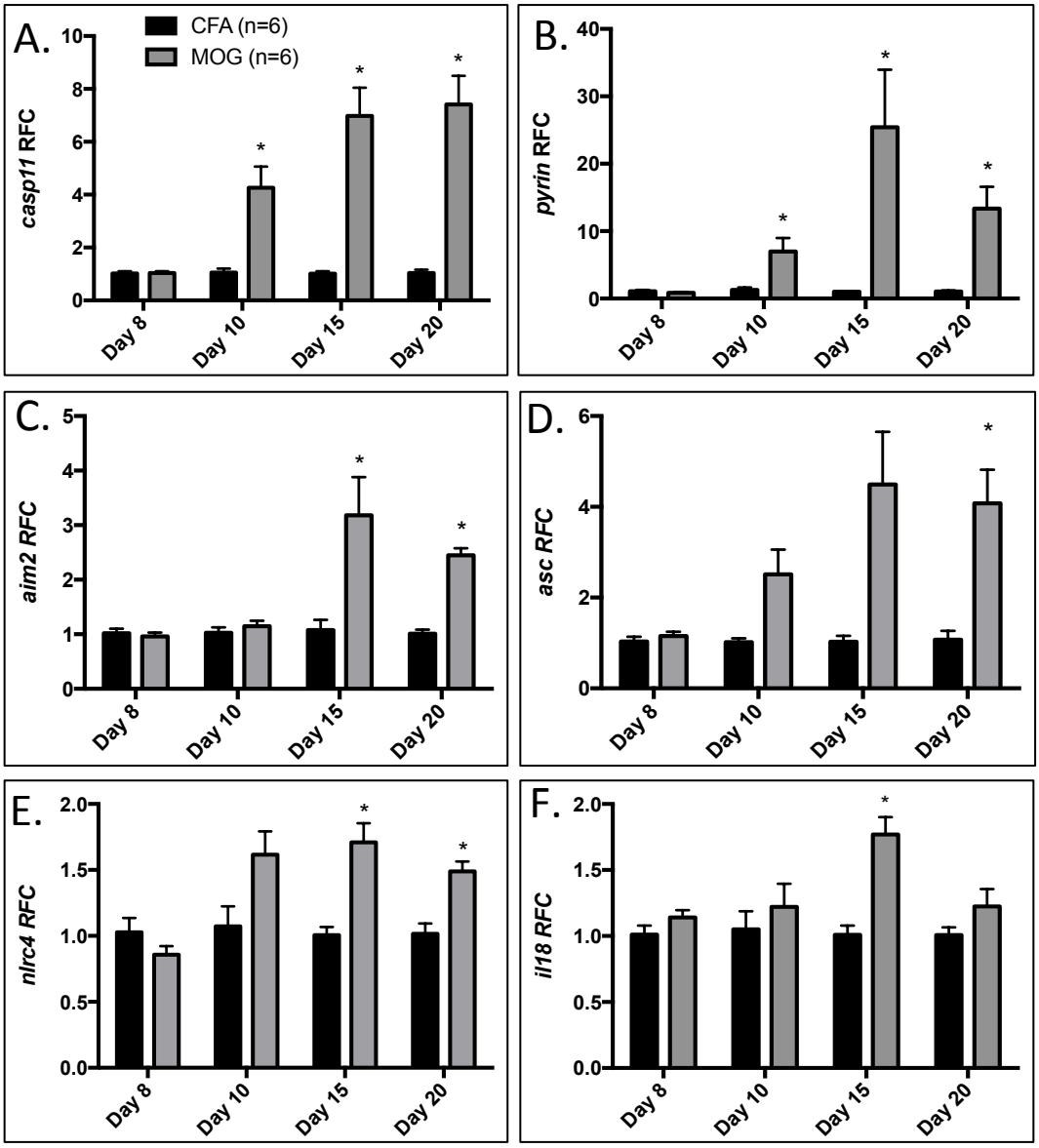

Supplemental Figure 9: Inflammasome gene expression in EAE
Control (CFA) and EAE (MOG) C57/Bl6 mice were induced on Day 0, and n=6 mice from each group were sacrificed on Day 8 (pre-onset), Day 10 (onset of neurobehavioural symptoms), Day 15 (mid-disease), and Day 20 (peak disease). Hindbrain transcript levels of (A) *casp11*, (B) *pyrin*, (C) *aim2*, (D) *asc,* (E) *nlrc4* and (F) *il18* were assessed using real-time RT-PCR. Levels of each transcript were significantly (Student's *t*-test, **p*<0.05) increased at various times throughout the disease course. Data represent relative fold change (RFC) compared to CFA controls, normalized to the housekeeping gene *hprt* (mean ± SEM).

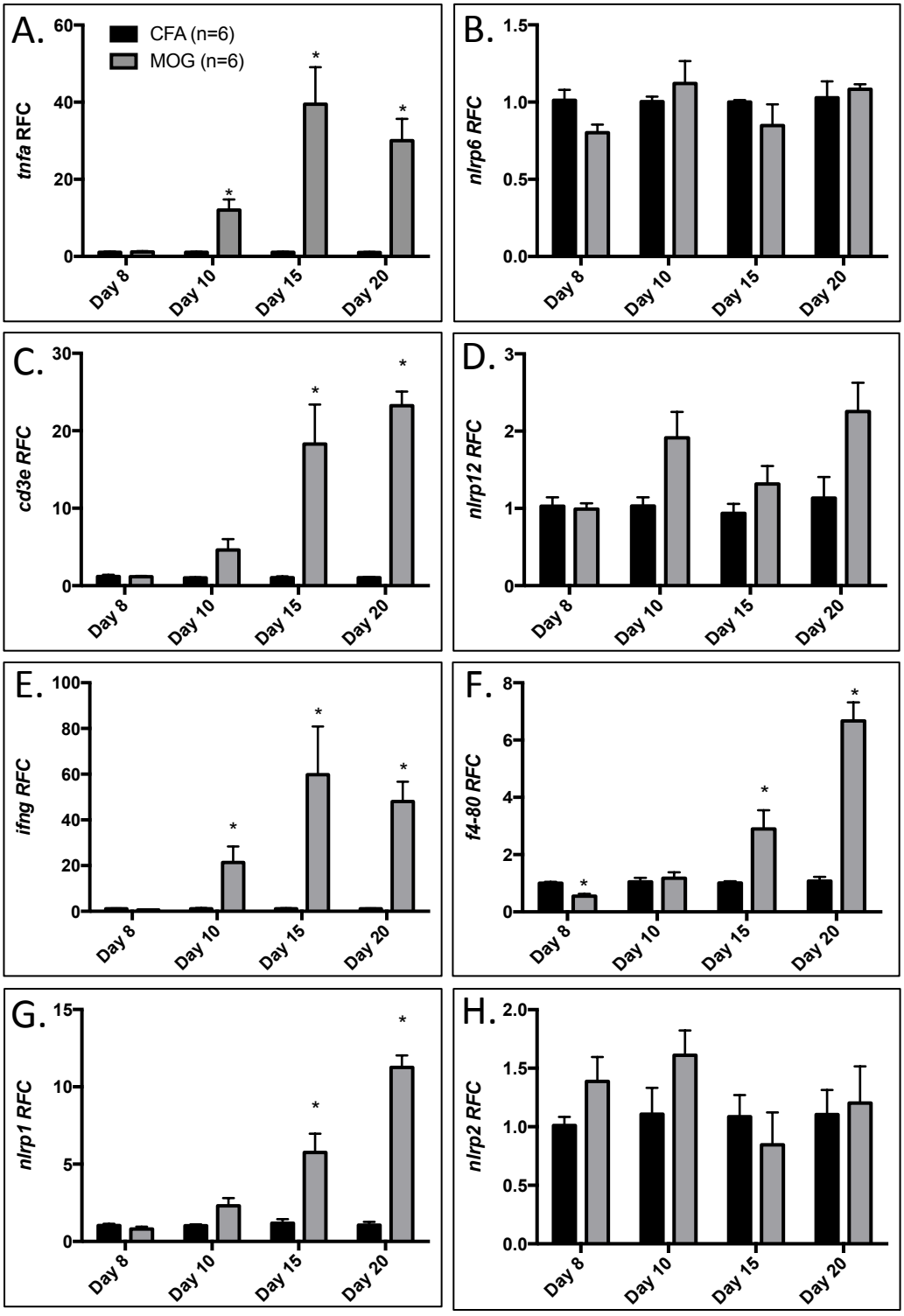

Supplemental Figure 10: Inflammasome gene expression over EAE disease course
Control (CFA) and EAE (MOG) C57/Bl6 mice were induced on Day 0, and n=6 mice from each group were sacrificed on Day 8 (pre-onset), Day 10 (onset of neurobehavioural symptoms), Day 15 (mid-disease), and Day 20 (peak disease). Hindbrain transcript levels of (A) *tnfa*, (B) *nlrp6*, (C) *cd3e*, (D) *nlrp12,* (E) *ifng* (F) *f480* (G) *nlrp1*, and (H) *nlrp2* were assessed using real-time RT-PCR. Levels of several transcripts were significantly (Student's t-test, *p<0.05) increased at various times throughout the disease course. Data represent relative fold change (RFC) compared to CFA controls, normalized to the housekeeping gene *hprt* (mean ± SEM).

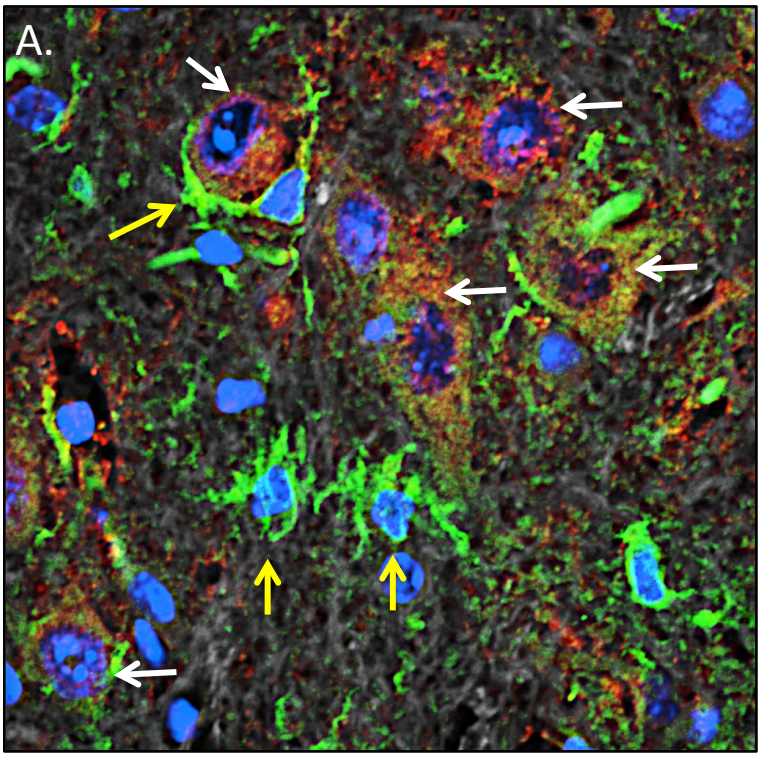

Supplemental Figure 11: *In vivo* microglial pyroptosis engages nearby microglia in spinal cord during EAE
(A) Immunofluorescent double-labelling of EAE lumbar spinal cord tissue at peak disease (Day 20) was performed to assess the localization of GSDMD (red) compared to myeloid cell marker Iba-1 (green) and GST-pi (grey-scale) in the white matter. This representative image illustrates the interaction between healthy microglia (indicated by yellow arrows; defined by Iba-1 expression [green] with intact processes and nucleus) and microglia undergoing pyroptosis (indicated by white arrows; defined by large dysmorphic nuclei [DAPI], GSDMD immunoreactivity [red], and diminished Iba-1 expression [green]. Healthy microglia that are $GSDMD^-$ are shown in close proximity to cells undergoing pyroptosis.

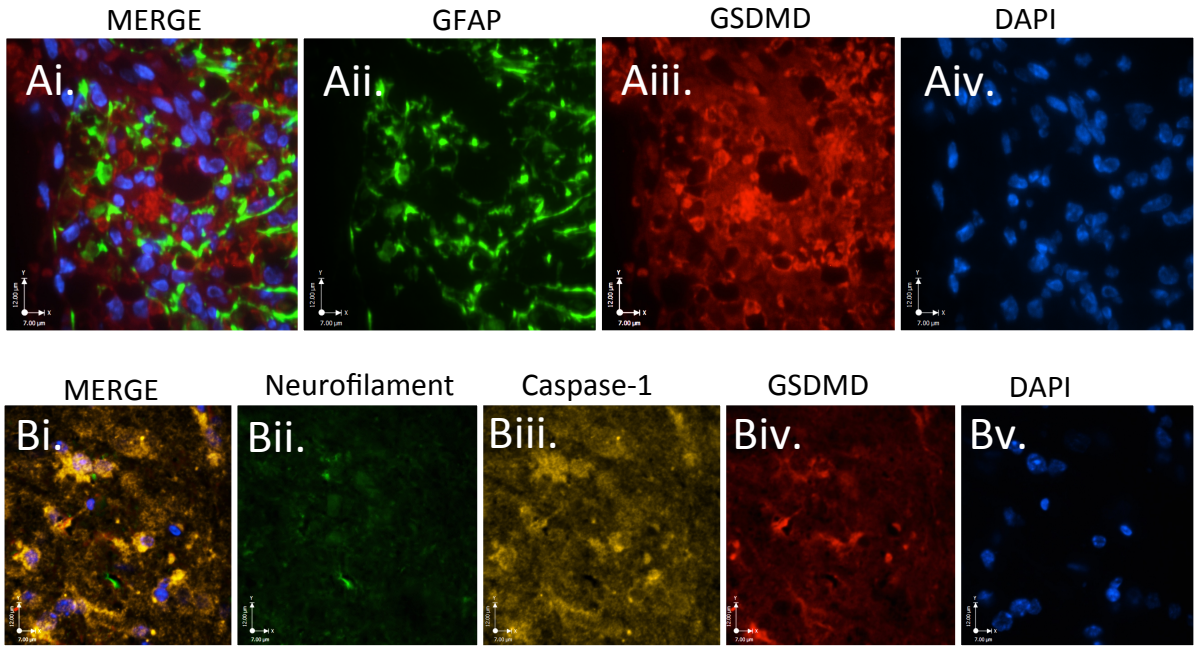

Supplemental Figure 12: Astrocytes and neurons do not co-express GSDMD in the ventral spinal cord of EAE animals

Immunofluorescent labeling of lumbar ventral spinal cord white matter from EAE animals sacrificed at peak disease (Day 20). (A) Astrocyte marker GFAP (Aii, green) and pyroptosis marker GSDMD (Aiii, red) do not co-localize within the same cells (merge, Ai) (B) Neuronal marker neurofilament (Bii, green) does not appear to colocalize with either caspase-1 (Biii, yellow) or GSDMD (Biv, red). Horizontal scale axis = 7μm and vertical scale axis =12μm.

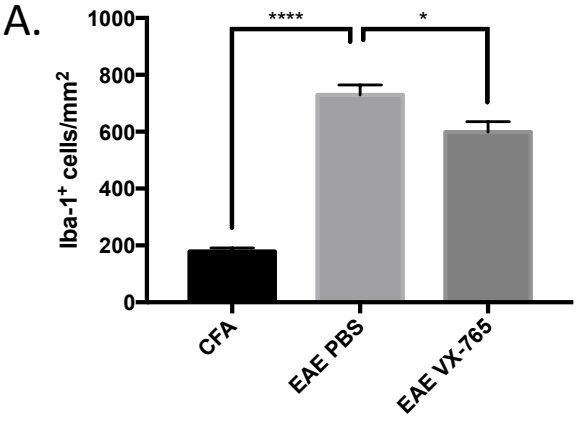

Supplemental Figure 13: Iba-1$^+$ microglia accumulate in EAE and are diminished with VX-765 treatment

(A) Lumbar spinal cords from control (CFA) and EAE mice treated with either vehicle (EAE +PBS) or VX-765 (EAE+VX-765) and sacrificed at peak disease were labelled with LFB to stain myelin and Iba-1 to label macrophages/microglia. The number of Iba1$^+$ cells in the ventral spinal column from CFA, EAE+PBS, and EAE+VX-765 animals was quantified (cells per mm^2). Immunohistochemical quantification was performed using multiple spinal cord sections from 2-3 animals per experimental condition, with a minimum of ten non-overlapping fields of view (FOV) per animal. Data shown represent mean cell number per mm^2 ± SEM and were tested for significance using 1-way ANOVA with Tukey's test for multiple comparisons (*p<0.05, ****p<0.001).

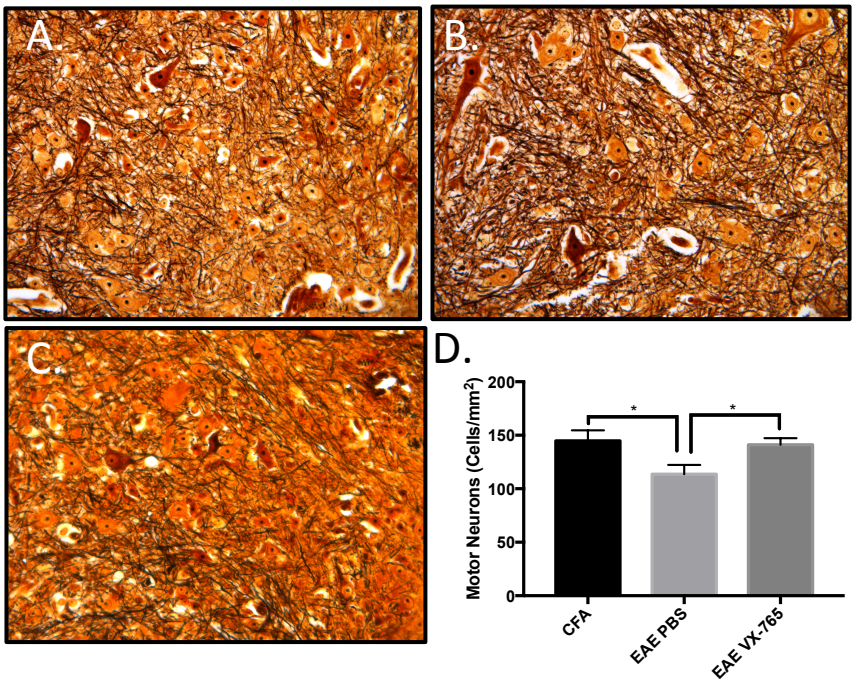

Supplemental Figure 14: **Preservation of motor neurons in the ventral spinal cord by VX-765**

(A) CFA, (B) EAE + PBS, and (C) EAE + VX-765 animals were sacrificed at peak disease (Day 20) and sections of the lumbar spinal cord were silver (Bielchowsky) stained. Motor neurons in the ventral horn were identified visually based upon a criteria of large triangular cell body and prominent nucleolus. (D) Data shown represent mean ± SEM (ANOVA with Tukey's multiple comparison tests, *p<0.05). n=2-3 animals per group, minimum of five discreet images per animal.

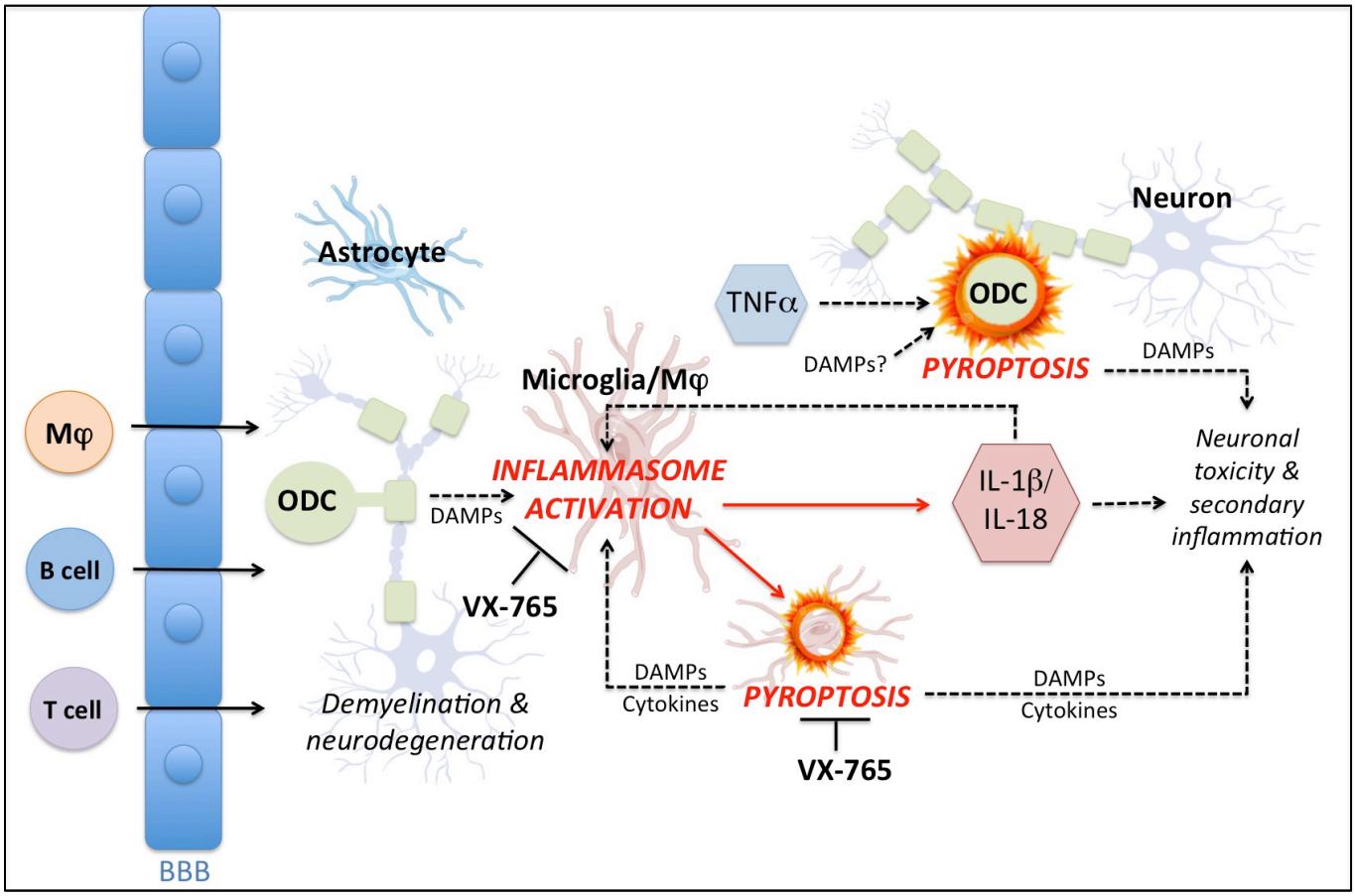

Supplemental Figure 15: Model of the inflammasome activation and pyroptosis cascade in MS
In MS and EAE, oligodendrocytes (ODCs) undergo an initial damaging event leading to demyelination/neurodegeneration, potentially driven by infiltrating peripheral immune cells, including T cells, B cells, and macrophages (Mφ). Dying ODCs and neurons release damage-associated molecular patterns (DAMPs), putative drivers of inflammasome activation in resident microglia and infiltrating macrophages. Activated brain myeloid cells (macrophages/microglia) release both non-inflammasome-associated (e.g. TNFα) and inflammasome-associated cytokines (IL-1β and IL-18). Secreted IL-1β and IL-18 act in autocrine/paracrine loops to drive local inflammasome activation, activate infiltrating lymphocytes, and cause direct neuronal toxicity. Inflammasome activation drives gasdermin-D (GSDMD)-mediated pyroptosis in brain myeloid cells. Pyroptosis leads to further release of DAMPs and inflammasome-associated cytokines, driving a secondary inflammatory cascade in the CNS. GSDMD upregulation and pyroptosis is also observed in ODCs, which may be driven by TNFα, putatively derived from activated microglia, or DAMPs in the local microenvironment. Although inflammasome-associated cytokines are not released from dying ODCs, pyroptosis may further exacerbate tissue damage and inflammation through direct loss of ODCs and release of DAMPs into the microenvironment. VX-765 directly blocks inflammasome activation through caspase-1 inhibition, thus reducing both the maturation/release of proinflammatory cytokines IL-1β and IL-18, and the maturation/activation of GSDMD. Through these actions, VX-765 reduces cytokine neurotoxicity, interrupts local inflammatory feedback loops, and prevents pyroptosis in multiple cell types, leading to tissue preservation and improved disease outcomes.

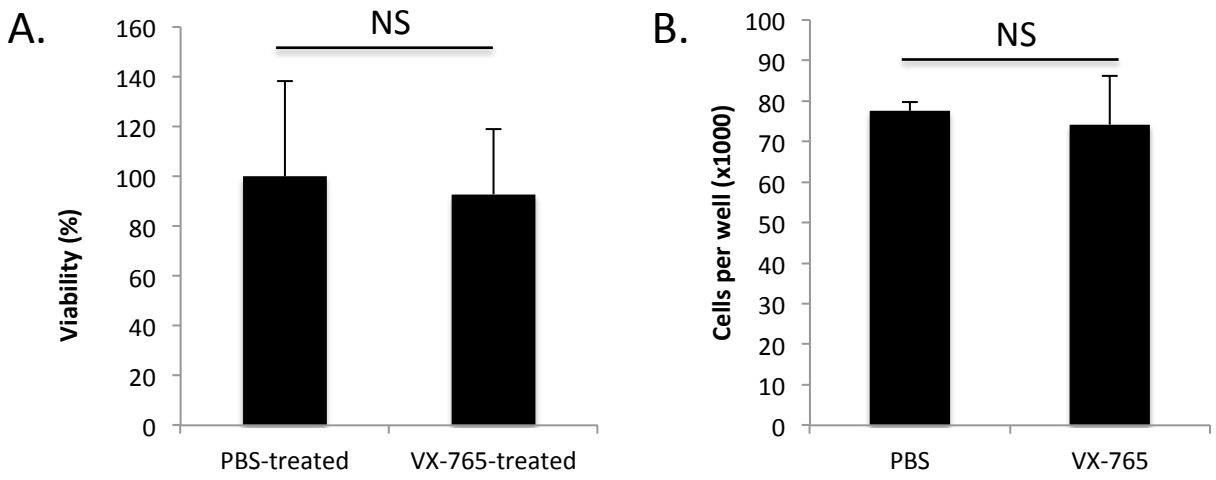

Supplemental Figure 16:
Human PBMC-derived lymphocytes were treated with VX-765 (50μM) or PBS (solvent control). Cytotoxicity was assessed by (A) Alamar Blue colorimetric assay, and (B) Trypan blue staining and counting at 24hrs post-treatment. Alamar Blue absorbance values were normalized to PBS-treated controls. Trypan blue values represent absolute cell numbers. Experiments were replicated with samples from two different tissue donors. Values shown represent mean ± SEM and were tested for significance using Student's *t*-test.

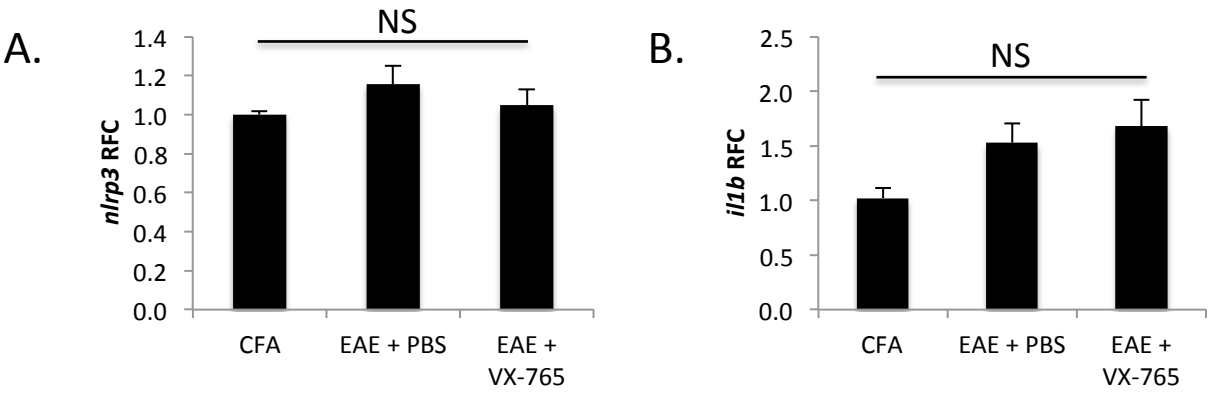

Supplemental Figure 17: **Inflammasome gene expression in spleen at peak EAE**
Spleens from CFA (n=6), EAE+PBS (n=9), and EAE+VX-765 (n=9) animals at peak disease were subject to RT-PCR to assess transcript levels of (A) *nlrp3* and (B) *il1b*. Data represent relative fold change (RFC) compared to CFA controls, normalized to the housekeeping gene *hprt.* Data shown are mean ± SEM and were tested for significance using ANOVA.

Supplemental Methods

***Primary cell cultures**:* Fetal brain tissues from 17-20 week fetuses were dissected, meninges were removed, and a single cell suspension was prepared through enzymatic digestion for 60 min with 2.5% trypsin and 0.2 mg/ml DNAse I, followed by titration through a 70-μm cell strainer. Cells were washed twice with fresh medium and plated in T-75 flasks. Cultures were maintained in MEM supplemented with 10% FBS, 2mM L-glutamine, 1mM sodium pyruvate, 1×MEM nonessential amino acids, 0.1% dextrose, 100 U/ml Penicillin, 100 μg/ml streptomycin, 0.5 μg/ml amphotericin B, and 20 μg/ml gentamicin. For microglial cells, mixed cultures were maintained for 1-2 weeks, at which point astrocytes and neurons formed an adherent cell layer with microglia loosely attached or free floating in the medium. Cultures were gently rocked for 20 min to resuspend the weakly adhering microglia in medium, which were then decanted, washed and plated. Purity of cultures was verified by immunofluorescence as previously reported by our group [3]. Progenitor-derived oligodendrocytes were cultured as previously described in growth factor-positive (GF^+) media [4]. Briefly, neural progenitor cells were cultured in DMEM/HAMS-F12 1:1 media with bovine serum albumin, L-glutamine, gentamicin, N2 components, and further supplemented with fibroblast growth factor (FGF), platelet-derived growth factor (PDGF-AA), Sonic hedgehog (Shh), triiodothyronine (T3), and neurotrophic factor 3 (NT-3) to generate pre-oligodendrocytes, referred to as undifferentiated oligodendrocyte progenitor cells. Cells were passaged when they reached 90-95% confluence. Final differentiation into mature oligodendrocytes was initiated by replacement of GF^+ media with identical media lacking the four growth factors (growth factor-negative media; GF^-). Expression of

oligodendrocyte progenitor markers (A2B5 and O-4) and differentiated oligodendrocyte markers (GalC and myelin basic protein) in undifferentiated and differentiated cultures respectively were validated previously [4].

***Western blot analysis**:* As previously described [3,5], primary human microglia were cultured for 4hr with the treatments indicated above at 37°C, 5% CO_2. Media was aspirated and plates washed twice with cold PBS. 1ml PBS was added to each well, and cells were detached using cell scrapers and transferred to 1.5mL microtubes, followed by centrifugation at 13,000 x g for 5min at 4°C. Pellets were dissociated and protein was isolated according to the Qiagen AllPrep DNA/RNA/Protein Mini Kit (80004) using ethanol-based protein precipitation followed by dissolution in Laemmli sample buffer for use in sodium dodecyl sulfate-polyacrylamide gel electrophoresis (SDS-PAGE). Protein samples were boiled in 95°C for 10min and stored at -20°C. Protein samples were separated using SDS-PAGE at 120V for 1hr on 12% mini-PROTEAN TGX™ precast gels (Bio-Rad, #456-1044). Proteins were transferred at 4°C onto nitrocellulose membranes (Hybond N; GE Healthcare) for 1hr. Membranes were blocked for 1hr in room temperature with Odyssey blocking buffer (Li-Cor Biosciences, Lincoln, NE, USA) to prevent nonspecific binding. Primary antibodies used included rabbit polyclonal caspase-1 p10 (1:1000, Santa Cruz Biotechnology, sc-514), rabbit polyclonal IL-1β (1:1000, Santa Cruz Biotechnology, sc-7884) and mouse monoclonal GSDMD (1:500, Abcam, ab57785). Membranes were probed with primary antibodies overnight at 4°C. Primary antibody binding was detected with peroxidase-conjugated secondary antibodies (goat anti-mouse IgG and goat anti-rabbit IgG from Jackson Immunoresearch) for 2hr at RT and developed using the Pierce™ ECL

Plus detection reagent (ThermoFisher, #32132). Bands were quantified where applicable using Image Studio rectangular analysis feature (LI-COR Biosciences). β-actin served as a loading control.

Cell culture immunofluorescence: As previously described [3], cells were cultured on 180μm thick polymer coverslip 8 well plates (μ-Slide ibiTreat plates #80826) and treated as appropriate. After 24hr, cells were fixed using 4% paraformaldehyde. Cells were permeablized using 0.1% Triton in PBS, blocked using Odyssey blocking buffer, and incubated with primary antibody overnight at 4°C. Primary antibodies used include rabbit polyclonal IL-1β (Santa Cruz Biotechnology, sc7884; 1:200; detects C-terminus of full-length and cleaved IL-1β), mouse monoclonal GSDMD (Abcam, 57785 1:100; raised against full-length GSDMD), and polyclonal caspase-1 (Santa Cruz Biotechnology, sc-514, 1:100; detects C-terminus of full-length and cleaved caspase-1). Primary antibody binding was detected using AlexaFluor 488 goat anti-rabbit IgG (Abcam, #ab150077; 1:500); AlexaFluor 647 goat anti-rabbit IgG (Abcam, ab150079; 1:500); or AlexaFluor 568 goat anti-mouse IgG (Abcam #ab175473; 1:500). Cells were stained with DAPI and mounted using Prolong™ Gold antifade reagent (Invitrogen, #P36934). F-actin staining was performed using ActinGreen™ 488 ReadyProbe reagent (Life Technologies, #R37110) according to manufacturer's instructions. Slides were imaged using a Wave FX spinning disc confocal microscope (Zeiss) with Volocity 6.3 acquisition and analysis software (Perkin Elmer).

Cell culture immunofluorescence quantification: Using Volocity 6.3 acquisition and analysis software, the intensity of each fluorescent channel was quantified by highlighting each individual cell to form a region of interest and recording the mean fluorescent intensity and area (μm^2) for each region of interest (ROI). *In vitro* images were taken on a single plane and no modifications were performed to images prior to analysis. Due to a higher background fluorescence observed in oligodendrocyte cell culture conditions, average MFI from no-primary controls was subtracted from raw MFI values. Microglial MFI values represent raw data with no subtraction. Cell length was measured using the line drawing feature of Volocity 6.3. Quantification was performed on a minimum of 100 cells per condition.

Quantification of pyroptotic bodies was performed using Volocity 6.3. A circular ROI was drawn overlaying each pyroptotic body and the mean fluorescent intensity (MFI) and area (μm^2) of each pyroptotic body calculated individually using the "measure" function. MFI of cytoplasm was calculated by selecting an ROI within the cell body that excluded pyroptotic bodies. Ratio of GSDMD immunoreactivity was calculated by dividing the MFI of each pyroptotic body by the MFI of the cytoplasm.

The formation of the "ring of fire" phenotype was defined by a rounded morphology, retraction of processes, and the formation of a ring of $GSDMD^+$ $IL\text{-}1\beta^+$ pyroptotic bodies on the cell membrane. Individual microglia were classified morphologically according to whether each cell met all of the "ring of fire" criteria. Where ambiguity existed in the

distribution of GSDMD in the cell, the histogram feature of Volocity was utilized to compare mean fluorescence intensity across the diameter of the cell.

Polymerase chain reaction (PCR): 1μg of total RNA was used for first-strand cDNA using Superscript II reverse transcriptase (Invitrogen, Carlsbad CA, USA) and with random hexamer primers (Roche). Specific genes were quantified by real-time reverse transcriptase PCR (RT-PCR) using i-Cycler IQ5 system (Bio-Rad, Mississauga, ON, Canada). The specific primers used in the real-time PCR are provided (Supplementary Tables 2 and 3). Semi-quantitative PCR analysis was performed by monitoring, in real time, the increase of fluorescence of the SYBR Green dye (iQ™ SYBR Green Supermix Bio-Rad) on the Bio-Rad detection system as previously reported [6], and was expressed as relative fold change (RFC) compared to untreated cell s and other-disease controls respectively.

Immunohistochemistry: Tissue sections were deparaffinized and hydrated using decreasing concentrations of ethanol. Antigen retrieval was performed by boiling the slides in 0.01M trisodium citrate buffer (pH 6.0) for 60 min. Endogenous peroxidases were inactivated by incubating sections in 0.3% hydrogen peroxide for 20 min. To prevent nonspecific binding, sections were preincubated with Odyssey buffer for 1 hr at room temperature. Primary antibodies used include rabbit polyclonal IL-1β (1:200, Santa Cruz Biotechnology sc7884), mouse monoclonal GSDMD (1:100, Abcam, 57785), rabbit polyclonal caspase-1 (1:100, Santa Cruz Biotechnology, sc-514), goat polyclonal pyrin (1:200, Santa Cruz Biotechnology, sc-30423), goat polyclonal GST-pi (1:500, Abcam ab53943), rabbit polyclonal Iba-1 (1:500, Wako, 019-19741), and mouse monoclonal MHC Class II (1:500,

Dako, M0775). Biotinylated secondary antibodies were utilized, and immunoreactivity detected using the Vectastain Avidin-Biotin Complex (ABC) kit (Vector Laboratories) with a 3,3'-diaminobenzidine tetrachloride (DAB) peroxidase substrate kit (Vector Laboratories). All slides were imaged using an upright microscope (Axioskop2; Zeiss MicroImaging Inc.).

Immunohistochemistry quantification: For human autopsy samples, immunohistochemical quantification was performed using a minimum of three MS and three nonMS (control) autopsy samples per protein of interest, with a minimum of six non-overlapping fields of view (FOV) per patient. For *in vivo* experiments, EAE and CFA animals were sacrificed at peak disease and sections of the lumbar spinal cord labeled for proteins of interest as described above. The number of IL-1β^+, caspase-1$^+$, and GSDMD$^+$ cells in the ventral spinal column was quantified (cells per mm^2) for multiple spinal cord sections from 2-3 representative animals per condition, with a minimum of ten non-overlapping fields of view (FOV) per animal. Cells were counted manually using the particle counting feature of ImageJ.

Motor neuron quantification: EAE and CFA animals were sacrificed at peak disease and sections of the lumbar spinal cord stained with silver (Bielchowsky) staining. Spinal cords were imaged at 40X and motor neurons in the ventral horn counted using the particle counting feature of ImageJ. Motor neurons in the ventral horn were identified visually based upon a criteria of large triangular cell body and prominent nucleolus.

Tissue Immunofluorescence: For mouse and human immunofluorescent studies, as described previously [5], tissue slides were de-paraffinized by incubation for 1hr at 60°C followed by one 10min and two 5min incubations in toluene baths through decreasing concentrations of ethanol to distilled water. Antigen retrieval was performed by boiling in 10mM sodium citrate (pH 6.0). Slides were blocked with HHFH buffer [1.0 mM HEPES buffer, 2% (v/v) horse serum, 5% (v/v) FBS, 0.1% (w/v) sodium azide in Hank's balanced salt solution (HBSS)] for 4 hours at room temperature. Slides were incubated with primary antibodies described above at 4°C overnight. Primary antibody was removed by PBS washes (5 min x3) and slides were incubated for 3min in 0.22μm filtered 1% (w/v) Sudan black in 70% ethanol and washed an additional three times in PBS. Slides were incubated in a mixture of 1:500 fluorescent secondary antibodies as appropriate for 2hr, washed three times in PBS, stained with DAPI for 10min, and mounted with Prolong Gold. Slides were imaged with an inverted Wave FX spinning disc confocal microscope (Zeiss).

Tissue immunofluorescence quantification: Using Volocity 6.3 acquisition and analysis software, spinal cords were imaged in z-stacks (6μm vertical distance) at a magnification of 40X. To quantify the number of positive cells in each channel, black levels were set at a strict threshold of triple the background MFI in every channel. Cells were considered positive if the signal exceeded this level and was associated with a distinct nucleus (DAPI). Cells were counted manually using the particle counting feature of Volocity.

Supplemental Methods References:

1 Schneider, C. A., Rasband, W. S. & Eliceiri, K. W. NIH Image to ImageJ: 25 years of image analysis. *Nature Methods* **9**, 671-675 (2012).

2 Branton, W. G. *et al.* Brain microbiota disruption within inflammatory demyelinating lesions in multiple sclerosis. *Scientific Reports* **6**, 37344, doi:10.1038/srep37344 (2016).

3 Walsh, J. G. *et al.* Rapid inflammasome activation in microglia contributes to brain disease in HIV/AIDS. *Retrovirology* **11**, 35, doi:10.1186/1742-4690-11-35 (2014).

4 Monaco, M. C. *et al.* Progenitor-derived oligodendrocyte culture system from human fetal brain. *Journal of Visualized Experiments : JoVE*, doi:10.3791/4274 (2012).

5 Boghozian, R. *et al.* Suppressed oligodendrocyte steroidogenesis in multiple sclerosis: Implications for regulation of neuroinflammation. *Glia*, doi:10.1002/glia.23179 (2017).

6 Maingat, F. G. *et al.* Neurosteroid-mediated regulation of brain innate immunity in HIV/AIDS: DHEA-S suppresses neurovirulence. *FASEB journal : official publication of the Federation of American Societies for Experimental Biology* **27**, 725-737, doi:10.1096/fj.12-215079 (2013).